



HAL
open science

Depth Evaluation of Curvilinear Cracks in Metal Using Multi-speed Laser Lock-in Thermography Method

C. Boué, S. Holé

► **To cite this version:**

C. Boué, S. Holé. Depth Evaluation of Curvilinear Cracks in Metal Using Multi-speed Laser Lock-in Thermography Method. *Journal of Nondestructive Evaluation*, 2022, 41 (2), pp.43. 10.1007/s10921-022-00875-0 . hal-04017894

HAL Id: hal-04017894

<https://hal.sorbonne-universite.fr/hal-04017894>

Submitted on 7 Mar 2023

HAL is a multi-disciplinary open access archive for the deposit and dissemination of scientific research documents, whether they are published or not. The documents may come from teaching and research institutions in France or abroad, or from public or private research centers.

L'archive ouverte pluridisciplinaire **HAL**, est destinée au dépôt et à la diffusion de documents scientifiques de niveau recherche, publiés ou non, émanant des établissements d'enseignement et de recherche français ou étrangers, des laboratoires publics ou privés.

Depth evaluation of curvilinear cracks in metal using multi-speed laser lock-in thermography method

C. Boué, S. Holé

Sorbonne Université, F-75005 Paris, France

LPEM, CNRS, ESPCI Paris, PSL Université, 10 rue Vauquelin, F-75005 Paris, France

christine.boue@espci.fr

ORCID

0000-0001-5412-3645

0000-0002-8921-1714

An original method using lock-in thermography with a laser excitation is proposed for the contactless estimation of open crack depths in metal with curvilinear shape. A continuous laser source regularly scans the structure under test leading to a periodical heating. The heat diffusion disturbances induced by a crack located in the thermal diffusion area are measured synchronously with the laser scans. The thermal signature of the crack is extracted from the amplitude of surface temperature images for various scanning speeds of the thermal source. The thermal signatures are analysed according to a length representative of the thermal diffusion length and to the radius curvature of the crack to give a local evaluation of the crack depth. The method, explained with 3D simulations, is experimentally implemented and tested with calibrated curvilinear cracks. The results demonstrate the potentiality of multi-speed laser lock-in thermography method as a contactless measurement tool for the evaluation of complex crack shapes up to 3 mm depth.

Keywords: Infrared thermography, lock-in thermography, non-destructive testing, crack depth, crack sizing, curvilinear crack.

1. Introduction

Mechanical stresses in metals can develop damaging cracks with complex profiles on surface and in depth. The active infrared thermography which analyses the disturbances of heat diffusion from a heat source is a non-contact and non-destructive technique widely used for the inspection of component [1]–[7]. However, the discontinuity of the heat diffusion which reveals the cracks depends also on parameters like the sample surface state, the crack width or the crack shape and the spatial configuration of the heating excitation [8]–[14]. Consequently, it is difficult to evaluate the crack depth, one of the most important parameters to assess the dangerousness of the crack, even for simple shape like linear cracks.

In [15] and [16] an original method using lock-in thermography is presented to directly evaluate linear open crack depths without requiring any calibration procedure. A moving punctual continuous heating spot is used as a 3D probe of the crack depth, adjusting its thermal diffusion length by its moving speed. At the same time, an infrared camera acquires surface temperature images in synchronism with the heating spot displacements. The evolution of the spatial derivatives of the amplitude images obtained from the surface temperature for different speeds is representative of the crack depth. It has been chosen in [16] to analyse the thermal response of an area back to the crack, in its “shadow”. This robust method is validated for simple linear crack shape but more complex crack shapes which represent an industrial issue must be analysed.

In this work, the method described in [16] is adapted to crack depth assessment for curvilinear geometry. Results from 3D Finite Element Method (FEM) simulation with COMSOL Multiphysics are used to introduce the adjustments required on crack indicators to take into account the crack curvature. These new developments applied for linear and curvilinear crack shapes are presented and analysed using the multi-speed laser lock-in thermography. They are then experimentally validated using thermo-erosion cracks of different curvature in steel samples.

2. Multi-speed laser lock-in thermography method

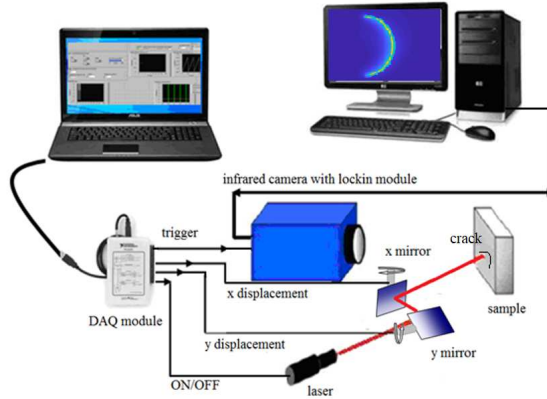


Fig. 1: experimental multi-speed lock-in thermography set-up

A continuous heating laser spot regularly moves along the crack from one end to the other on a distance L with speed v (Fig.1). At the end of the path, the heating source is switched off to return back to its initial position as quickly as possible and restarts (switched on) its movement along the crack. Each heated point sees the thermal source periodically (a few periods) during a short time compared to the duration L/v . The thermal source moves in this way for several speeds (usually 5 speeds are sufficient). The heating source has to be located near the crack so that the crack acts as a thermal barrier which modifies locally the heat diffusion. In the case of non-linear crack shapes, the surface temperature distribution, which depends on the thermal diffusivity D of the studied material, is also sensitive to the crack shape curvature. Indeed, the heating spot can be on the concave or convex side of the crack. Consequently, the different speeds of the heating source along the crack must be correctly chosen. The thermal diffusion length μ used as a 3D scan parameter is:

$$\mu = \sqrt{\frac{DL}{\pi v}} = \sqrt{\frac{D\Delta t}{\pi}} \quad (1)$$

where Δt is the source displacement duration for speed v for one scan.

The acquisition process of the infra-red camera is synchronized by an external trigger signal (Fig. 1) that is activated when the laser spot returns to its initial position. The camera lock-in module generates the amplitude and phase images of the surface temperature at the trigger frequency. In the absence of a lock-in module, for instance in the case of simulations, the amplitude and phase images are calculated by Fast Fourier Transform (FFT) of a series of surface images acquired during one scan of the heat source. One amplitude and one phase images are then extracted from the first harmonic ($f_0=1/\Delta t$) of the FFT calculation for each heat source displacement speed.

The crack signature is extracted from the amplitude image A_{sh} of an area located in the crack shadow area where heat diffusion and thus the surface temperature on the sample have been impaired after bypassing the crack (Fig. 2). The maximum value μ_{max} of μ has to be chosen larger than the distance d between the heat spot and the crack.

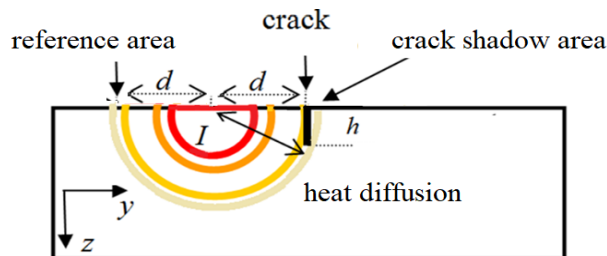


Fig. 2: sample model in cross section (y,z directions). The heat source is located on the left side of the crack and the crack shadow is located on the right side of the crack. d is the distance from the heat source to the crack and h is the crack depth.

In the procedure described in [16], a depth indicator is obtained from the ratio between the temperature in the crack shadow area and a reference temperature measured symmetrically to the heat path which corresponds indeed to the temperature expected in the crack shadow area in case of the absence of the crack. The depth indicator has a poor dependency on the crack width if it is sufficiently small compared to crack depth [15,16]. In the case of curved cracks, the reference and the shadow points must be determined according to geometrical considerations. Fig. 3 illustrates the two geometrical possibilities depending on whether the heating spot is in the concave or convex side of the crack path.

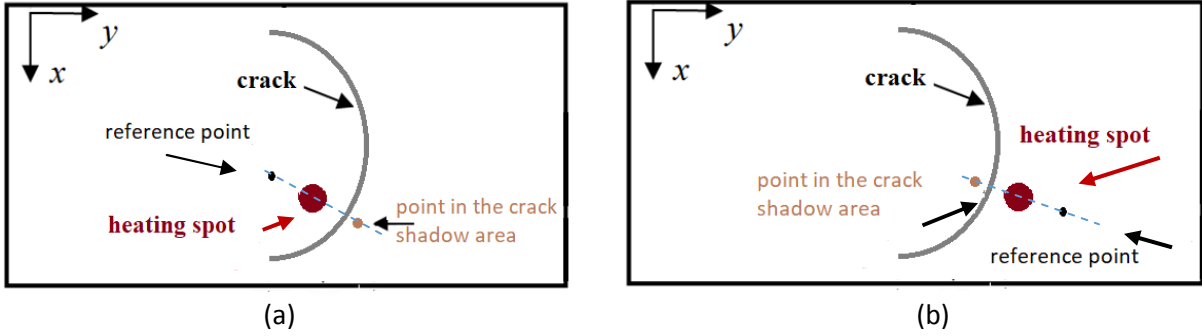


Fig. 3: top view of the sample model (x,y directions). The heating spot is located (a) on concave side or (b) on convex side of the crack path. The crack shadow is located behind the crack on a line perpendicular to the crack path and passing through the heating spot. The reference point is located on the same line, symmetrically to the crack shadow point with respect to the heating spot.

Tetrahedral meshing is adapted to the different domains (bulk, crack) of the studied samples for the 3D Finite Element Method (FEM) simulations made with COMSOL Multiphysics. The number of mesh elements depends on the size of the crack (depth and width). It is between 250 000 and 800 000 for depths between 0.5 mm to 3 mm and for width of 200 μm or 50 μm . 100 surface temperature images are calculated during a scan and 5 scans are performed with 5 different speeds. Fig.4a shows a typical mesh in (x,y,z) directions in case of a curvilinear crack of 20-mm curvature radius and 2-mm crack depth. Fig.4b represents the calculated infrared amplitude image A using a continuous moving heat spot ($\Delta t = 16$ s and $L = 55$ mm). The curved crack footprint is clearly visible at the right of the moving heat source. Each crack pixel P extracted from the spatial derivative of the amplitude image is associated with 3 aligned pixels: its local heat source which is its nearest hottest pixel, its reference and its shadow pixels. The crack shadow pixel is chosen at a distance Δd_{sh} of a few pixels Δp_{sh} from P in the shadow area. The reference pixel is at the distance $d + \Delta d_{sh}$ from the local heat source. Fig. 4c shows the localizations of the maximum heating positions (in green), the crack (in blue), the reference area (in black) and the shadow area for $\Delta p_{sh} = 4$ pixels (in red). Δp_{sh} value can be chosen as convenient to get rid of the pixel noise at the crack positions and to obtain a sufficient signal.

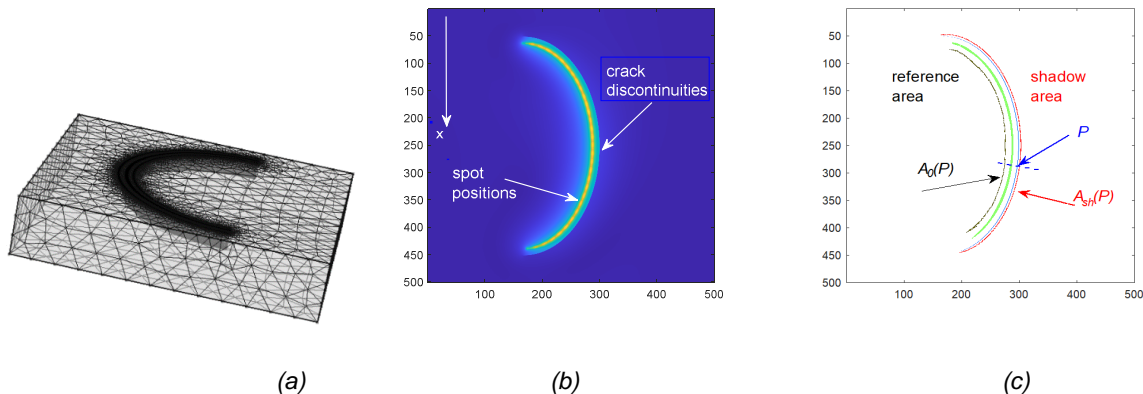


Fig. 4: (a) surface mesh in (x,y,z) directions used for FEM simulations in case of curvilinear crack, (b) simulated amplitude images A (arbitrary units a.u.), (c) Localisation image of crack pixels (in blue), hottest (in green), reference (in black) and shadow pixels (in red) extracted from simulated amplitude image. 1 pixel represents 100 $\mu\text{m} \times 100 \mu\text{m}$. Simulated crack $h = 2$ mm, width = 200 μm , $L = 55$ mm. Distance of the heat source to the crack $d = 1.25$ mm, radius of the heat source $r = 0.25$ mm, thermal diffusivity $D = 4.5e^{-6} \text{m}^2/\text{s}$, displacement duration of moving continuous heat source $\Delta t = 16$ s, number of pixels for the probing area definition $\Delta p_{sh} = 4$ pixels.

The shadow amplitude $A_{sh}(P)$ and the reference amplitude $A_0(P)$ of the selected pixels P are defined for each speed values. $A_{sh}(P)$ depends on the crack geometry, the heating area and the speed of the heating spot whereas $A_0(P)$ does not depend on the crack depth.

3. Crack indicators for depth evaluation

Four samples with a curvilinear crack of 20-mm radius and with a constant depth (0.5 mm, 1 mm, 2 mm, 3 mm) are simulated. The shadow amplitude $A_{sh}(P)$ and the reference amplitude $A_0(P)$ of selected pixels are extracted from the calculated amplitude images obtained for different speeds. Fig. 5 shows A_{sh}/A_0 curves (5 speeds) and their polynomial fits f_h as a function of normalized thermal diffusion length μ/μ_{max} . μ_{max} is the maximum value of the chosen thermal diffusion lengths μ . Each depth is identified by a well differentiated curve (color). The line bundle obtained for each depth in the simulations is mainly a consequence of the uncertainty of the calculated temperatures resulting from the meshing and the time sampling.

It was chosen in [16] to extract from the fits two specific points called I_A and I_B indicators. The indicator I_A , which can be defined as $I_A = 1 - (A_{sh}/A_0)_{max}$ for $\mu = \mu_{max}$ represents the thermal energy measured behind the crack at long time. The indicator I_B represents the reduced thermal diffusion length at which the heat begins to bypass the crack. I_B corresponds to the value μ/μ_{max} when $f_h = s$, s being generally chosen as a decreasing linear function of μ/μ_{max} ; here, $s = 1 - \mu/\mu_{max}$.

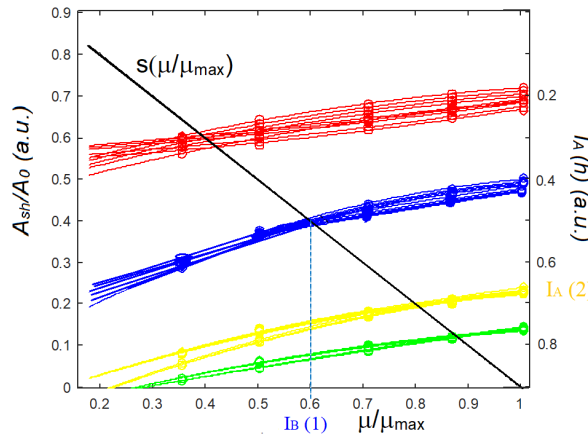


Fig. 5: A_{sh}/A_0 and their fits as a function of μ/μ_{max} for simulated depth values $h = 0.5$ mm (in red), $h = 1$ mm (in blue), $h = 2$ mm (in yellow), $h = 3$ mm (in green) for 10 selected pixels P . The abscissa of the intersection of A_{sh}/A_0 and the line $s(\mu/\mu_{max})$ in black gives the indicator I_B for the crack depth. The value $1 - (A_{sh}/A_0)_{max}$ at $\mu/\mu_{max} = 1$ gives the indicator I_A for the crack depth. Simulated parameters: maximum of the thermal diffusion length is $\mu_{max} = 4.7$ mm; number of pixels for the probing area definition is $\Delta p_{sh} = 4$ pixels;

Finally, to improve the robustness of the depth evaluation, the global crack indicator is calculated with:

$$I = I_A \cdot I_B \quad (2)$$

Fig. 6 presents the indicator I calculated with (4) as a function of the x pixel position of 300 selected pixels along the crack for 4 constant depths. (The crack extremity pixels are not considered). These curves show the good sensitivity of indicator I to the crack depth although the indicator seems to slightly depend on the crack position, more importantly for larger depth.

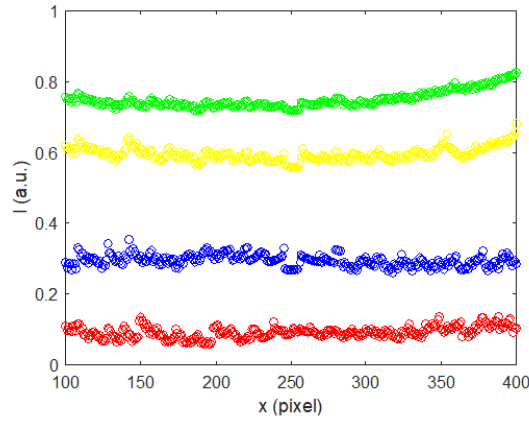


Fig. 6: Indicator I (arbitrary unit) along the crack (pixels in x direction) of a curvilinear crack (radius 20 mm) for 4 depth h values (0.5 mm in red, 1 mm in blue, 2 mm in yellow, 3 mm in green). The heating displacement is in the concave area. 1 pixel represents 100 μm .

4. Geometry considerations for depth evaluation in case of curvilinear crack shapes

In order to assess the impact of the crack curvature, the multi-speed laser lock-in thermography method is applied to various curvilinear crack shapes. The presented simulated results are calculated using a moving continuous heat spot along a curved crack shape with a constant crack depth h . In these simulations, the crack width is chosen equal to the presented experimental artificial crack width (200 μm).

4.1 Localisation of the heating spot with respect to crack curvature

In case of a curvilinear curve, the heating spot can be positioned at a distance d on the convex or on the concave crack side. Fig. 7 shows the simulated amplitude images for a 20 mm radius curved crack.

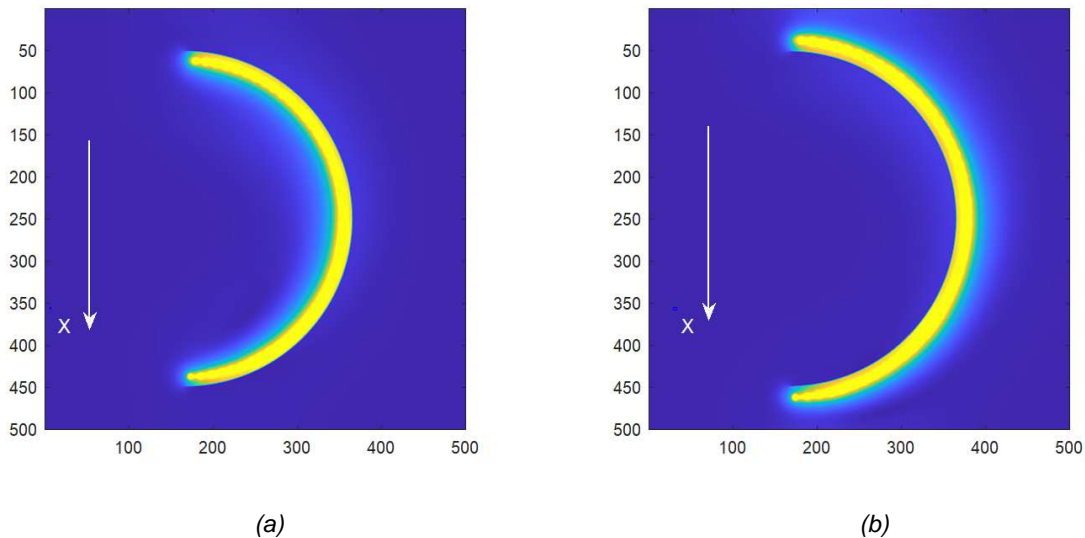


Fig. 7: Infrared simulated amplitude image A. (a): concave configuration, (b): convex configuration. The simulated depth is $h = 2\text{mm}$. 1 pixel represents 100 $\mu\text{m} \times 100 \mu\text{m}$. The crack curvature is 20 mm. The distance of the heat source to the crack is $d = 1.25\text{mm}$. The number of pixels for the probing area definition is $\Delta p_{sh} = 4$ pixels. The thermal diffusivity is $4.5 \times 10^{-6} \text{m}^2/\text{s}$.

In Fig. 8, A_{sh} (in blue) and A_0 (in red) are extracted along the x direction for 5 heating spot speed (Δt between 2 s to 16 s) for the selected pixels along the crack for the concave (Fig. 8a) or the convex (Fig. 8b) heating configuration. In the concave configuration (Fig. 8a), A_0 is higher and A_{sh} is slightly lower than in the convex configuration (Fig. 8b). Consequently, A_{sh}/A_0 is lower for the concave configuration.

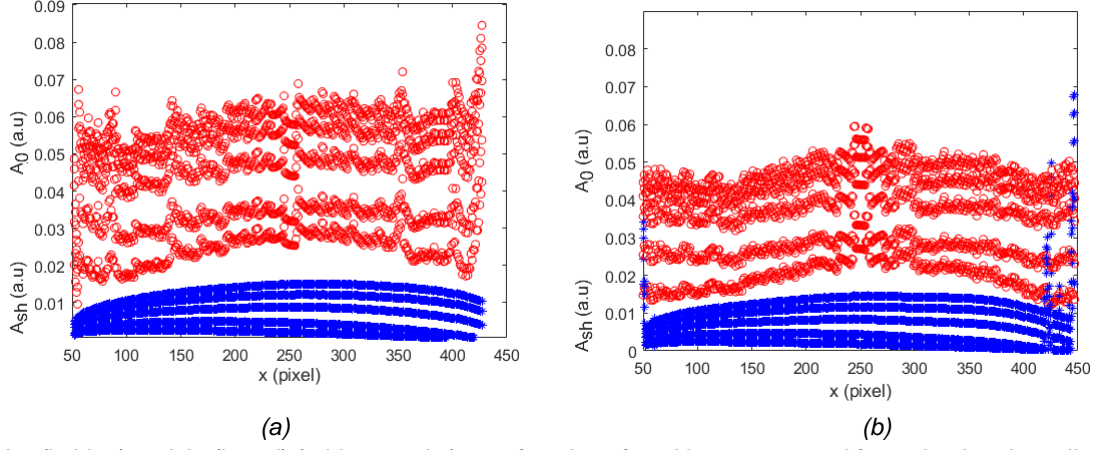


Fig. 8: A_{sh} (in blue) and A_0 (in red) (arbitrary units) as a function of position x , extracted from simulated amplitude images obtained for 5 spot speeds. (a): heating spot in the concave area. (b): heating spot in the convex area. Simulated depth $h = 2\text{ mm}$. 1 pixel in x direction represents $100\mu\text{m}$. The distance of the heat source to the crack is $d = 1.25\text{ mm}$. The crack curvature is 20 mm . The number of pixels for the probing area definition is $\Delta p_{sh} = 4$ pixels. The thermal diffusivity is $4.5 \cdot 10^{-6}\text{ m}^2/\text{s}$.

Consequently, the resulting I indicator is higher if the heating spot is in concave configuration compared to that obtained in convex configuration. The model might not be suitable when the heating spot is in convex configuration, for example when A_{sh}/A_0 is near or greater than 1.

I indicators obtained for the concave and convex configurations are presented Fig. 9 for two d distances. Calculated I obtained for the heating spot in a concave configuration (in blue) leads to better differentiation of depths. In the convex configuration (in red), I indicator loses sensitivity for small crack depth and greatly depends on distance d compared to the concave configuration.

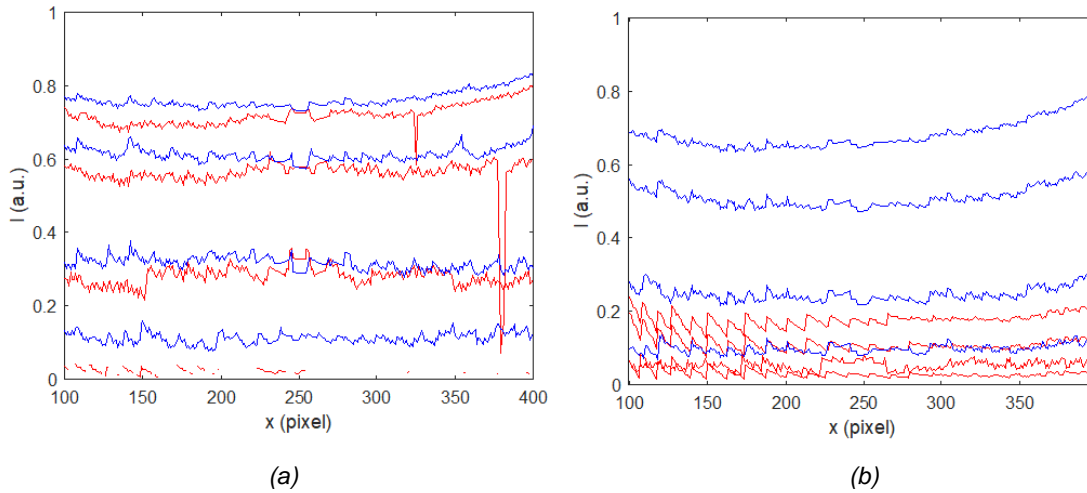


Fig. 9: indicator I (a.u.) as a function of x position (pixel) for curvilinear crack shapes for 4 crack depths ($h = 0.5\text{ mm}$, $h = 1\text{ mm}$, $h = 2\text{ mm}$, $h = 3\text{ mm}$) and for concave configuration (in blue) and convex configuration (in red). (a) distance $d = 1.25\text{ mm}$. (b) distance $d = 2\text{ mm}$.

Fig. 10 presents more specifically the concave and convex mean responses with $d = 2\text{ mm}$ which is the distance of the experimental results presented thereafter.

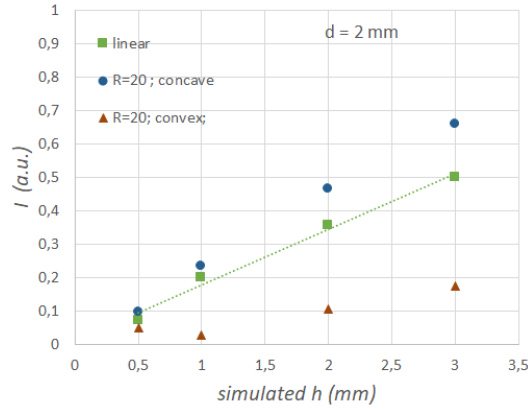


Fig. 10: indicator I (a.u.) as a function of simulated crack depth (mm) for a 20 mm curvilinear crack shapes (heating spot in a concave configuration (in blue) and in a convex configuration (in brown)). The linear line is the fitting curve for the linear crack response (in green). The distance $d = 2$ mm.

For a distance of 2 mm (Fig. 10), I obtained in the convex heating position (in brown) are underestimated compared to those obtained for a linear configuration (in green). Conversely, I obtained for the concave heating position (in blue) are overestimated.

4.2 Radius of the curvilinear crack

The surface amplitude is simulated with different crack curvatures ($R = 10$ mm, $R = 20$ mm, infinity R). Fig. 11 compares the I indicator obtained from linear (infinity R) and curvilinear heating displacements (which amounts to saying linear or curvilinear crack shapes) obtained for $d = 1.25$ mm. Fig 11 shows that the I values obtained for the curved crack (extracted from Fig. 9) are overestimated compared to those obtained for a linear crack. Furthermore, the indicator values are higher for the concave heating compared to those obtained with the convex heating. These observations show the I dependence to the crack geometry in x,y directions and that a geometrical correction has to be taking into account.

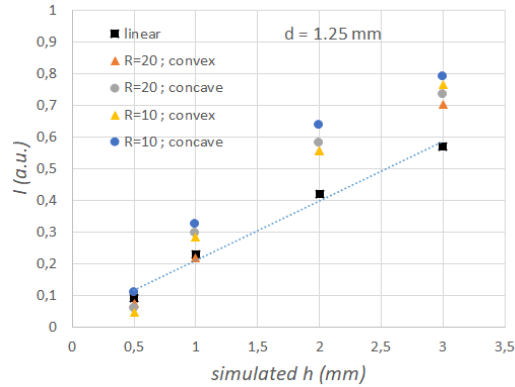


Fig. 11: indicator I (a.u.) for linear and curvilinear crack shapes as a function of crack depths (mm) for different heating configuration (convex or concave). The linear line is the fitting curve for the linear crack response. The crack radius is $R = 20$ mm or $R = 10$ mm, the distance is $d = 1.25$ mm.

The results obtained for the concave configuration better differentiate the different depths. Thus they are used afterwards to determine a basic geometrical correction. The chosen geometric factor takes into account the radius of curvature of the heated area ($R-d$) as well as the distance between the heating area and the shadow area ($d+d_{sh}$). The most suitable geometric model is the square function. For a large radius of curvature, the model tends to the linear model.

The depth evaluation h_{ev} is deduced from the indicator I using only the concave results by:

$$h_{ev} = I \left(1 - \frac{d + d_{sh}}{R - d} \right)^2 G \quad (3)$$

where G is the correction deduced from the slope of the linear response (line in Fig. 11). Since the indicator depends little on the crack opening [16], G is virtually independent of the crack width.

Fig. 12 shows the evaluated depth obtained using (5). The G value deduced from the linear (infinity R) response is equal to 5 for $d = 1.25 \text{ mm}$ and 6 for $d = 2 \text{ mm}$ for material whose thermal diffusivity is close to the one of steel. These simulated results obtained for curvilinear crack ($R = 10 \text{ mm}$ and $R = 20 \text{ mm}$) validate the method for curvilinear cracks. The proposed geometrical correction for the depth indicators is efficient if the heating spot is localised in the crack concave area.

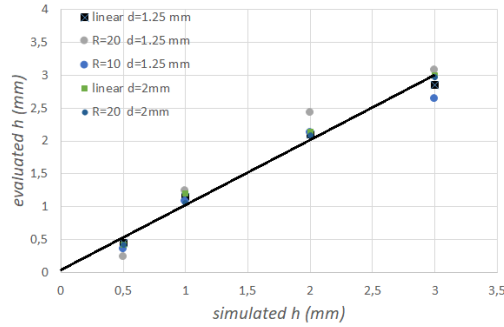


Fig. 12: depth evaluation (mm) as a function of simulated h (mm) for the non-constant linear crack and for curved constant cracks ($R=10 \text{ mm}$ and $R=20 \text{ mm}$) with $G = 5$ for $d = 1.25 \text{ mm}$ and $G = 6$ for $d = 2 \text{ mm}$. The black line corresponds to the expected response.

5. Experimental results

Experimental tests were carried out to access to the depth evaluation of artificial vertical open cracks made by electro-erosion in steel cubes. Four steel samples have a curvilinear crack of radius 20 mm with a constant depth (0.5 mm, 1 mm, 2 mm, 3 mm). One sample is a steel block with a linear crack with no constant 0-4 mm depth. The measured thermal diffusivity of the plate [13] is equal to $4.5 \pm 0.3 \cdot 10^{-6} \text{ m}^2 \text{ s}^{-1}$. The shape of the cracks is necessary to correctly position the laser spot and to determine the local radius of curvature necessary for the geometric correction. In this study, the crack shapes are well identified. A prior localization step is therefore not necessary. In less favorable cases, the image of the crack location obtained without optimizing the position of the laser [17], provides the necessary information both to adjust the trajectory of the laser spot and to determine the local radius of curvature of the crack.

Using the multi-speed laser lock-in method, the experimental results are obtained from 5 amplitude infrared images of 5 laser displacement speeds (L scanned in 2 s to 16 s). The experimental parameters (speed v and distance d) depend on the sample thermal diffusivity and on the power of the thermal source. The thermal diffusion length μ is obtained by (1). The thermal sensitivity of the method is better for low speed which induces maximum thermal length μ_{max} , but the synchronous acquisition process may shift near DC measurements.

Fig. 13 to 15 show the amplitude images obtained for a sample with a curvilinear crack and for the sample with a linear crack. The laser is positioned in the concave area of the crack curve (Fig. 13), in the convex area (Fig. 14) or near the linear crack (Fig. 15). Fig. 13b, Fig. 14b and Fig. 15b show the localization of the crack pixels, the hottest, normalized and shadow pixels extracted from measured amplitude image (Fig. 13a, Fig. 14b and Fig. 15b).

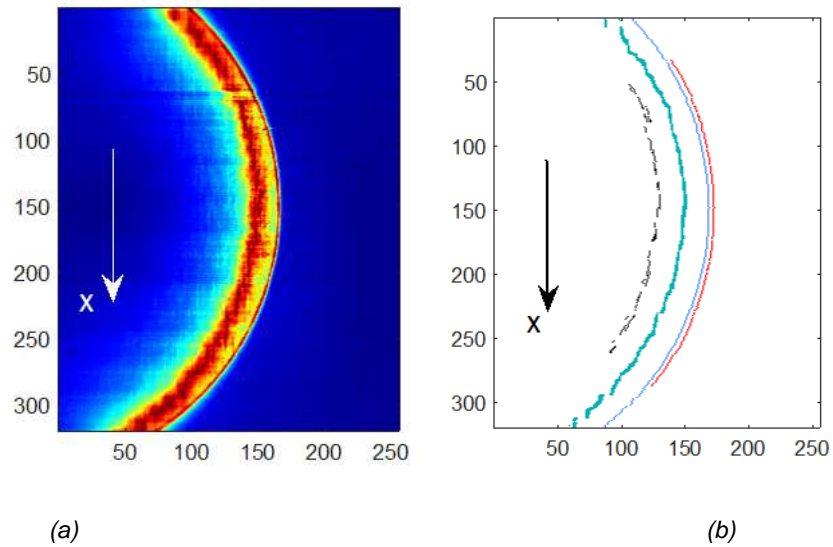


Fig. 13: heating displacement along the concave side of the curvilinear crack, (a) amplitude images A (arbitrary units a.u.), (b) localisation of crack pixels (in blue), hottest (in green), reference pixels (in black) and shadow pixels (in red) extracted from measured amplitude image. 1 pixel represents $100 \mu\text{m} \times 100 \mu\text{m}$. The crack width is $200 \mu\text{m}$ and crack depth is $h = 2 \text{ mm}$. Thermal diffusivity is $D = 4.5 \text{ e}^{-6} \text{ m}^2/\text{s}$. Displacement duration of moving continuous heat source is $\Delta t = 16 \text{ s}$. Number of pixels for the probing area definition is $\Delta p_{sh} = 4$ pixels.

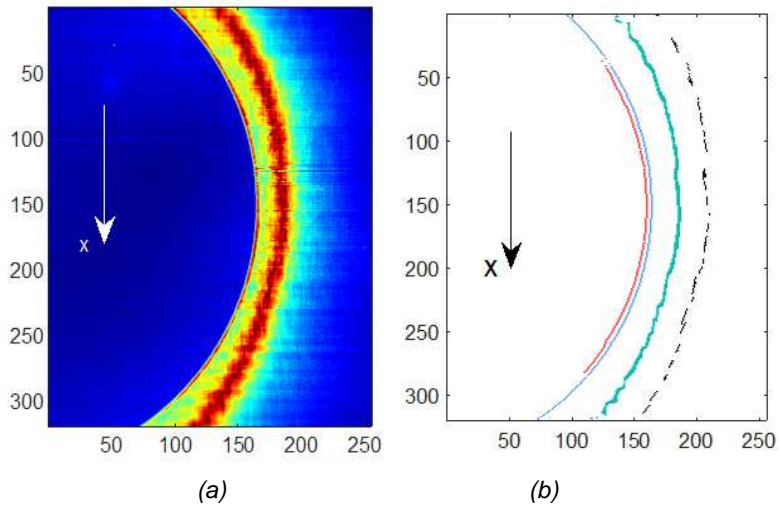


Fig. 14: heating displacement along the convex side of the curvilinear crack, (a) amplitude images A (arbitrary units a.u.), (b) localisation of crack pixels (in blue), hottest pixels (in green), reference pixels (in black) and shadow pixels (in red) extracted from measured amplitude image. 1 pixel represents $100 \mu\text{m} \times 100 \mu\text{m}$. The crack width is $200 \mu\text{m}$ and crack depth is $h = 2 \text{ mm}$. Thermal diffusivity is $D = 4.5 \text{ e}^{-6} \text{ m}^2/\text{s}$. Displacement duration of moving continuous heat source is $\Delta t = 16 \text{ s}$. Number of pixels for the probing area definition is $\Delta p_{sh} = 4$ pixels.

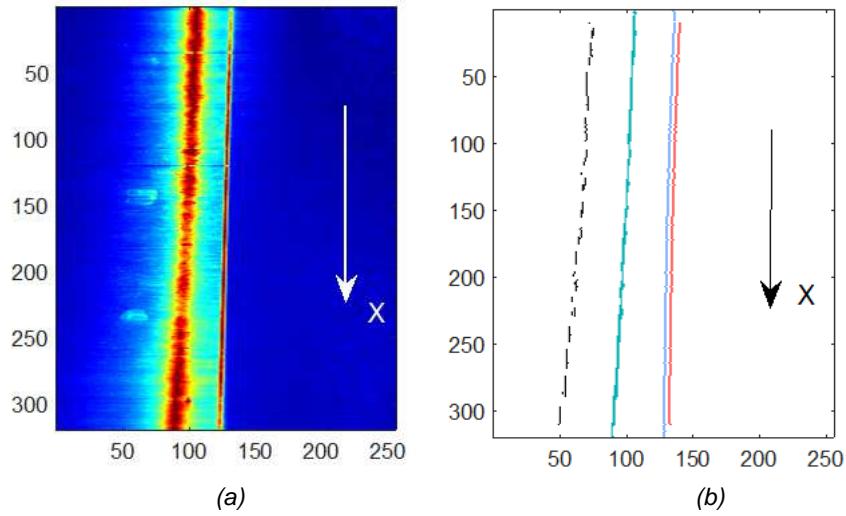


Fig. 15: heating displacement along a linear crack, (a) amplitude images A (arbitrary units a.u.), (b) localisation of crack pixels (in blue), hottest pixels (in green), reference pixels (in black) and shadow pixels (in red) extracted from measured amplitude image. 1 pixel represents $100 \mu\text{m} \times 100 \mu\text{m}$. The crack width is $200 \mu\text{m}$ and crack depth $h = 0.5\text{-}3.5 \text{ mm}$. Thermal diffusivity is $D = 4.5 \cdot 10^{-6} \text{ m}^2/\text{s}$. Displacement duration of moving continuous heat source is $\Delta t = 16 \text{ s}$. Number of pixels for the probing area definition is $\Delta p_{sh} = 4$ pixels.

The presented process is first validated using the linear crack with a non-constant depth. The I indicator responses calculated using (2) are presented Fig. 16. The G value deduced from the slope of the line is equal to 6 which corresponds more or less to the one obtained by simulation.

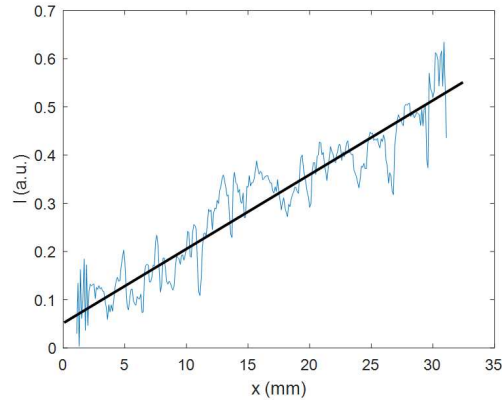


Fig. 16: indicator I (a.u.) as a function of x displacement (mm) for a non-constant $0.5\text{-}3.5 \text{ mm}$ crack depth. The black line corresponds to the linear response. Laser power $P = 2 \text{ W}$. Studied length along the crack $\Delta x = 30 \text{ mm}$.

Fig. 17 shows the A_{sh}/A_0 curves (5 measurements and their fits) for the four steel samples having a curvilinear crack from which are extracted the indicators I_A and I_B . Fig. 17a, the heating laser spot in in concave area: the depth information is relevant. Fig. 17b, the heating laser spot in the convex area: the depth information is lost for shallow depths.

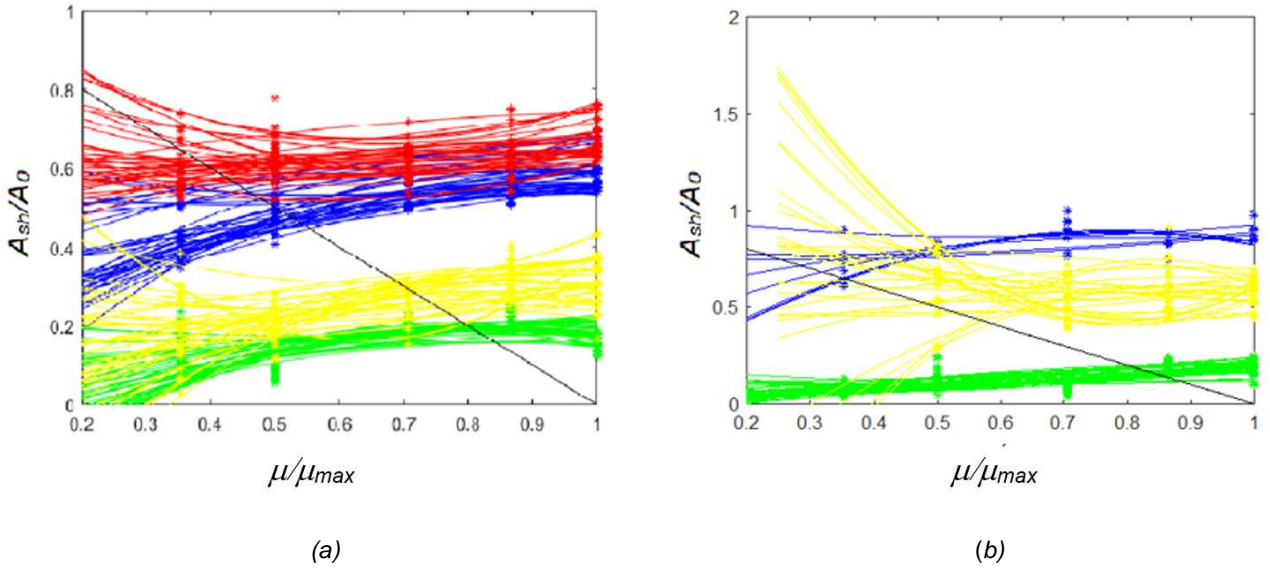


Fig. 17: A_{sh}/A_0 measurements and their fits (a.u.) as a function of μ/μ_{max} for crack depth values $h = 0.5$ mm (in red), $h = 1$ mm (in blue), $h = 2$ mm (in yellow), $h = 3$ mm (in green) for 40 selected P pixels. The intersection of an A_{sh}/A_0 curve and the line $s(\mu/\mu_{max})$ in black gives the I_B indicator of the crack depth. The value $1 - (A_{sh}/A_0)_{max}$ at $\mu/\mu_{max} = 1$ gives the I_A indicator of the crack depth. (a): concave configuration, (b): convex configuration. Maximum of the thermal diffusion length $\mu_{max} = 4.8$ mm. Number of pixels for the probing area definition $\Delta p_{sh} = 4$ pixels. Laser power 2W.

The post processing procedure extracts I_A and I_B indicators from Fig. 17a to calculate I indicator following (2) (Fig. 18).

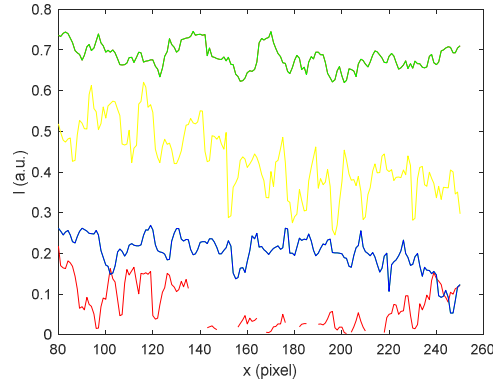


Fig. 18: indicator I (a.u.) along the crack (x direction) of curvilinear crack for four h values (0.5 mm in red, 1 mm in blue, 2 mm in yellow, 3 mm in green) in case of a concave configuration of the heating spot.

The depth evaluation (Fig. 19) is calculated from (3) with $G = 6$ for 4 depth values extracted from the linear crack responses ($h = 0.5$ mm, $h = 1$ mm, $h = 2$ mm, $h = 3$ mm) and for the 4 depth values of the curvilinear cracks in case of a concave heating spot configuration.

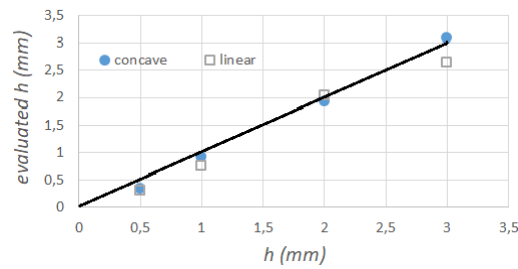


Fig. 19: crack depth evaluation (mm) as a function of h (mm) for the non-constant linear crack (4 measurements) and for the curvilinear constant depth electro erosion “cracks” with a heating spot displacement on the concave side of the crack. Width of the cracks $200\ \mu\text{m}$, $G = 6$. The black line corresponds to the expected response.

With a 2W continuous laser power and a high sensitivity infrared camera, the multi-speed laser lock-in method allows to evaluate 0-3 mm crack depth for linear crack as well as for curvilinear crack. The total camera acquisition duration is around 2 min for 5 multi-speeds lock-in method.

6. Conclusion

The multi-speed lock-in infrared thermography method is an experimental method which allows to evaluate linear and curvilinear crack depth, independently of their width.

The evolution of the depth indicator is analysed by simulations for curvilinear crack. The simulation results allow to propose a simple geometrical correction to take into account the crack curvature in the calculations of depth evaluations. Measurements with an infrared camera obtained with linear and controlled curvilinear “cracks” in steel blocks validate the proposed indicator for curvilinear shapes. The geometrical correction is made on simple cases of curvilinear cracks with constant radius of curvature. For more complex geometries, it is then necessary to take into account local radii of curvature. Taking into account the shape of the crack allows to study cracks other than linear.

The multi-speed lock-in infrared thermography method evaluates cracks of a few centimetre long. This method is indicated for the investigation of curvilinear geometries as long as the displacement of a laser beam onto the surface is possible. No surface preparation and no calibration procedure are required. The depth evaluation method is non-polluting, non-destructive and is implemented with simple optical adjustments.

Declarations: to be used for all articles, including articles with biological applications

Funding: not applicable

Conflicts of interest/Competing interests: not applicable

Availability of data and material (data transparency) : all data and materials support the published claims and comply with field standards.

Code availability (software application or custom code) : not applicable

Authors' contributions : not applicable

Additional declarations for articles in life science journals that report the results of studies involving humans and/or animals : not applicable

Ethics approval : This work has not been published before, is not under consideration for publication anywhere else, and the publication has been approved by all co-authors

Consent to participate : all the co-authors consent to submit and they obtained consent from the responsible authorities at the institute/organization where the work has been carried out.

Consent for publication : all the co-authors consent for publication.

REFERENCES

- [1] S. A. Shifani, P. Thulasiram, K. Narendran, and D. R. Sanjay, “A Study of Methods using Image Processing Technique in Crack Detection,” in *2020 2nd International Conference on Innovative Mechanisms for Industry Applications (ICIMIA)*, Mar. 2020, pp. 578–582, doi: 10.1109/ICIMIA48430.2020.9074966.

- [2] B. Oswald-Tranta, S. Feistkorn, G. Rössler, and M. Scherrer, "Comparison of different inspection techniques for fatigue cracks," in *Thermosense: Thermal Infrared Applications XLII*, Apr. 2020, vol. 11409, p. 114090C, doi: 10.1117/12.2556853.
- [3] U. Netzelmann, G. Walle, S. Lugin, A. Ehlen, S. Bessert, and B. Valeske, "Induction thermography: principle, applications and first steps towards standardisation," *Quant. InfraRed Thermogr. J.*, vol. 13, no. 2, pp. 170–181, Jul. 2016, doi: 10.1080/17686733.2016.1145842.
- [4] D. A. Exarchos, K. Dassios, and T. E. Matikas, "Novel infrared thermography approach for rapid assessment of damage in aerospace structures," in *Smart Materials and Nondestructive Evaluation for Energy Systems IV*, Mar. 2018, vol. 10601, p. 106010P, doi: 10.1117/12.2300171.
- [5] F. Ciampa, P. Mahmoodi, F. Pinto, and M. Meo, "Recent Advances in Active Infrared Thermography for Non-Destructive Testing of Aerospace Components," *Sensors*, vol. 18, no. 2, p. 609, Feb. 2018, doi: 10.3390/s18020609.
- [6] D. Balageas *et al.*, "Thermal (IR) and Other NDT Techniques for Improved Material Inspection," *J. Nondestruct. Eval.*, vol. 35, no. 1, p. 18, Mar. 2016, doi: 10.1007/s10921-015-0331-7.
- [7] N. Barakat, J. Mortadha, A. Khan, B. A. Abu-Nabah, M. O. Hamdan, and S. M. Al-Said, "A one-dimensional approach towards edge crack detection and mapping using eddy current thermography," *Sens. Actuators Phys.*, p. 111999, May 2020, doi: 10.1016/j.sna.2020.111999.
- [8] A. Mohan and S. Poobal, "Crack detection using image processing: A critical review and analysis," *Alex. Eng. J.*, vol. 57, no. 2, pp. 787–798, Jun. 2018, doi: 10.1016/j.aej.2017.01.020.
- [9] A. Salazar, A. Mendioroz, and A. Oleaga, "Flying spot thermography: Quantitative assessment of thermal diffusivity and crack width," *J. Appl. Phys.*, vol. 127, no. 13, p. 131101, Apr. 2020, doi: 10.1063/1.5144972.
- [10] J. González, A. Mendioroz, and A. Salazar, "Flying-spot thermography: sizing the thermal resistance of infinite vertical cracks," in *Thermosense: Thermal Infrared Applications XLI*, Baltimore, United States, May 2019, p. 20, doi: 10.1117/12.2523247.
- [11] K. Li, Z. Ma, P. Fu, and S. Krishnaswamy, "Quantitative evaluation of surface crack depth with a scanning laser source based on particle swarm optimization-neural network," *NDT E Int.*, vol. 98, pp. 208–214, Sep. 2018, doi: 10.1016/j.ndteint.2018.05.011.
- [12] J. Qiu, C. Pei, H. Liu, and Z. Chen, "Quantitative evaluation of surface crack depth with laser spot thermography," *Int. J. Fatigue*, vol. 101, pp. 80–85, Aug. 2017, doi: 10.1016/j.ijfatigue.2017.02.027.
- [13] B. Oswald-Tranta, "Time and frequency behaviour in TSR and PPT evaluation for flash thermography," *Quant. InfraRed Thermogr. J.*, vol. 14, no. 2, pp. 164–184, Jul. 2017, doi: 10.1080/17686733.2017.1283743.
- [14] Z. Shi, X. Xu, J. Ma, D. Zhen, and H. Zhang, "Quantitative Detection of Cracks in Steel Using Eddy Current Pulsed Thermography," *Sensors*, vol. 18, no. 4, p. 1070, Apr. 2018, doi: 10.3390/s18041070.
- [15] C. Boué and S. Holé, "Open crack depth sizing by multi-speed continuous laser stimulated lock-in thermography," *Meas. Sci. Technol.*, vol. 28, no. 6, p. 065901, 2017.
- [16] C. Boué and S. Holé, "Comparison between multi-frequency and multi-speed laser lock-in thermography methods for the evaluation of crack depths in metal," *Quant. InfraRed Thermogr. J.*, pp. 1–12, 2019.
- [17] Y. Fedala, M. Streza, F. Sepulveda, J.-P. Roger, G. Tessier, C. Boué, "Infrared lock-in thermography crack localization on metallic surfaces for industrial diagnosis," *Journal of Non Destructive Evaluation*, DOI 10.1007/s10921-013-0218-4, 2013